A Novel Device Model Validation Strategy for 1.5 T and 3 T MRI Heating Safety Assessment

Yu Wang, Shuo Song, Jianfeng Zheng, *Member, IEEE*, Qingyan Wang, Stuart A.Long, *Life Fellow IEEE*, Wolfgang Kainz, *Member, IEEE*, and Ji Chen, *Senior Member, IEEE*.

Abstract—**This paper presents a novel test instrument and strategy for active implantable medical device (AIMD) model validation under a radio-frequency (RF) field generated by a magnetic resonance imaging (MRI) system. A high electric field generator is developed as an alternative instrument for standard MRI RF coils. This system is both compact and power efficient. In addition, a set of validation pathways are proposed based on the Hadamard matrix. These pathways provide low correlations among incident electric fields and yet generate relative high temperature rises. Two generic AIMDs with different lengths are used to validate the strategy experimentally. It is demonstrated that this method provides an efficient and effective alternative for future AIMDs model validation under MRI RF emissions.**

Index Terms—**Active implantable medical device (AIMD), device model validation, high electric field generator, orthogonality, uncertainty.**

I. Introduction

MAGNETIC resonance imaging (MRI) examination is a common procedure used in hospitals today. For patients implanted with an active implantable medical device (AIMD), such as a neuro-stimulator or a deep brain stimulator, there is an increased demand to undergo MRI scanning. Since these devices often have long and insulated electrodes (lead body), they can act as a receiving antenna to collect the radiofrequency (RF) induced energy generated by the MRI RF coil and deposit the collected energy into the human tissue at the tip electrodes. Consequently, these localized energy depositions can lead to temperature rises near the tip electrode and may cause tissue damage[1]–[4].

To understand the mechanism of RF-induced heating, both numerical simulations and rigorously designed experiments were performed in recent years[5]–[9]. Since it is challenging to perform comprehensive modeling of an AIMD with sub-millimeter features in large heterogeneous media[10], [11], a transfer function concept was proposed to model the performance of AIMD exposed to RF fields, [12], [13]. The transfer function for the lead model, referred to as the AIMD electrode model, relates the incident field on the device to the induced heating at the tip electrodes. Combined with the incident electric field, the transfer function can be utilized to predict the in-vivo RF-induced heating for AIMD along all possible implanted pathways inside the human body during the MRI procedure [14].

However, due to the numerical approximations and imperfections of the electromagnetic model of AIMD, the experimental validation of the theoretical result is necessary[15]. The ISO/TS 10974 standard requires this transfer function model to be validated extensively before one can apply this for a clinically relevant study [16]. In the validation, the directly measured temperature rises and predicted temperature rises using the transfer function model along these pathways should be compared against each other. If the differences between the predicted temperature rises and directly measured results are less than the test uncertainty, the transfer function model is considered to be validated. This procedure of comparing the measured results with those predicted by the transfer function method is referred to as the transfer function model validation test.

Designing the lead trajectories is critical for the model validation test in terms of effectiveness and robustness. Effectiveness is mainly determined by the orthogonality of the tangential electric field along the trajectories; while the robustness is related to the ability to produce relative high temperature rises so that the measured signal-to-noise ratio can be large. The ISO/TS 10974 standard presents some suggested lead trajectories including changes in magnitude, phase, or combinations of magnitude and phase in Annex M[16]. However, electric fields along those trajectories are highly correlated, which could lead to two different transfer function models yielding similar temperature rises since the number of degrees of freedom existing in the incident electric field is insufficient [17]. Also, it is very complicated to practically achieve, and also inconvenient as well since rectangular, elliptical, and circular phantoms are needed. For 1.5 T and 3 T systems, different RF coils are required which will increase the difficulty of the test efforts significantly.

In this paper, a novel validation test strategy employing highly orthogonal electrical field distributions along pathways in a designed electric field generating system is proposed. The inspiration for the pathway is from the Hadamard matrix, which already has a broad application in telecommunications and statistics .[18]–[20]. The electric field generating system is a rectangular resonator operating at either 64 MHz or 128 MHz, which are the resonant frequencies for 1.5 T and 3 T MRI

Yu Wang, Shuo Song, Jianfeng Zheng, Qingyan Wang, Stuart Long,and Ji Chen are with the Department of Electrical and Computer Engineering, University of Houston, TX 77204-4005 USA (e-mail: ywang129@uh.edu; ssong11@uh.edu; jzheng4@central.uh.edu; qwang25@uh.edu; long@uh.edu; jchen23@central.uh.edu)

W. Kainz is with the Center for Devices and Radiological Health, Food and Drug Administration, Silver Spring, MD 20852 USA (e-mail: wolfgang.kainz@fda.hhs.gov).

systems, respectively. It can present a stable and homogeneous electric field with linear polarization over a large volume, and therefore provide an ideal environment to implement a high orthogonal electric field distribution along different pathways, as well as lowering the uncertainty due to the pathway shift. The entire system to perform the transfer function validation test for AIMDs is much smaller than the MRI RF coil. More significantly, it is capable of performing the validation tests for both 1.5 T and 3 T systems [21]. It should be pointed out that this paper focuses on the model validation using temperature rises at AIMD tip electrode. It is assumed here that the power deposition near the tip electrode would be directly related to the temperature rises near the electrode tip.

This remainder of this paper is organized as follows. In Section II, the design and implementation of a multi-frequency electric field generator, along with the pathway development methodology, are illustrated. Two AIMDs with different lengths are used as examples to show their validity and feasibility in Section III. Then the proposed strategy is compared with that of ISO 10974 to demonstrate the advantage of orthogonality of the electric field distribution along different pathways and accuracy due to the field homogeneity, in Section IV. Finally, conclusions are discussed in Section V.

II. METHOD

The transfer function is a numerical model to predict the RF-induced heating for AIMDs that are implanted in human tissue. It can be measured by a vector network analyzer (VNA) together with a current probe when assigning a radiating dipole at the lead tip [13], [14]. With the incident electric field tangential to the lead implantation trajectories when the lead is absent, the transfer function can accurately predict the temperature rises under specific RF field exposure, using

$$\Delta T = \left|\int_L TF(l)E_{\tan}(l)dl\right|^2, \quad (1)$$

where $TF(l)$ is the transfer function of the AIMD with units of $\mathrm{m}\cdot\sqrt{℃}/\mathrm{V}$, and $E_{\tan}$ is the incident electric field tangential to the lead pathway with units of V/m. ΔT is the temperature rise with units of ℃. To ensure the AIMD model is accurate, $TF(l)$ shall be validated along the predesigned incident electric field pathways per the ISO 10974 standard. The electric field distributions should be similar to those in real MRI scanning environments, to ensure the measurable temperature rises. Besides, as requested by ISO/TS 10974 8.8, “The selected incident fields for the validation shall be sufficiently different than the incident field(s) used for generating the AIMD model, and the difference shall be justified[16].” Also, “The tangential electric field exposure set for validation shall include changes in magnitude, phase or combinations of magnitude and phase, at different locations spanning the length of the AIMD.” Therefore, the electric fields along these pathways should be independent to others to satisfy the effectiveness of the validation test.

A. Multi-frequency electric field generator design

A high electric field generator that resonates at both 64 MHz and 128 MHz is proposed to substitute for the MRI RF coil to perform the validation test. As shown in Fig. 1, the signal generator, the power amplifier, the four-way Wilkinson power divider with pre-matching circuits, and the resonator constitute the high electric field generating system.

The sine or square wave coming from the signal generator is amplified by a power amplifier with gain of 50 dB. The matching circuit consisting of lumped elements adjusts the impedance seen by the input of the power divider to 50 Ω. It consists of two separate sets of circuitry for each frequency. The high power signal is divided into four ways with identical phase and magnitude. The special four-way feeding network is achieved by exciting the front (+z) and back (-z) walls respectively of the cavity as shown in Fig. 1 below. The resonator has dimensions of 30 cm by 30 cm. The height of the gel, with relative permittivity of 78 and conductivity of 0.47 S/m, is 9 cm [22], [23]. With the boundary condition of a PEC on the surrounding four planes (±x and ± z) and a PMC on the gel-air interface (±y), the resonator supports the TE10 mode at 64 MHz, as well as the TE10 and TE12 modes at 128 MHz [21]. The simulated electric field distribution at both frequencies is depicted in Fig. 2.

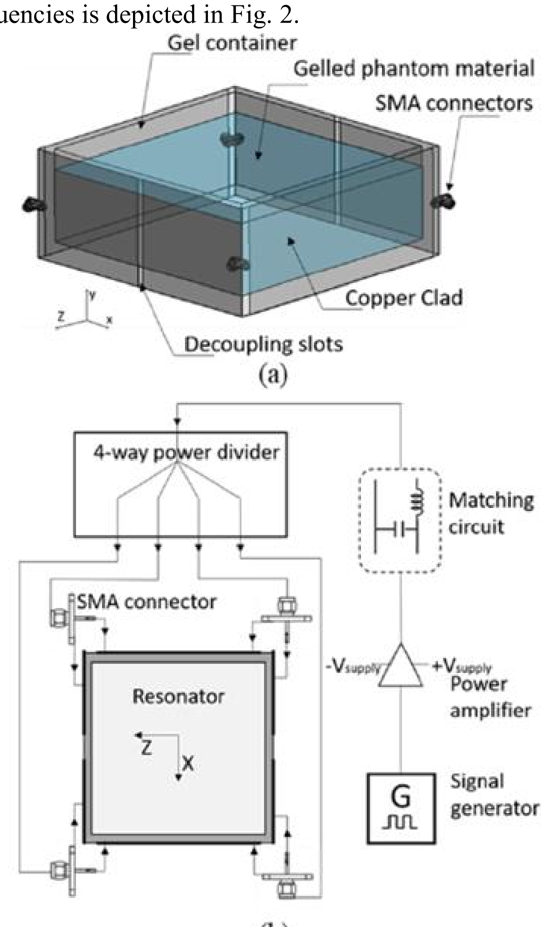

Fig. 1. The high electric field generating system. (a) The resonator structure working at both 64 MHz and 128 MHz; (b) The entire system configuration.

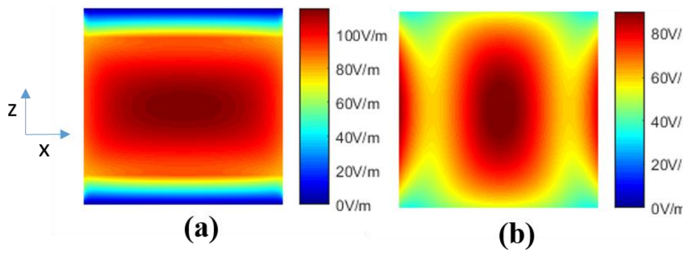

Fig. 2. Simulated electric field distribution on the center slice of the gel (a) at 64 MHz and (b) at 128 MHz with an input power of 32.52 W and 13.77 W, respectively.

The electric field distribution has been validated both by numerical simulation and experiment using a 10 cm titanium rod [21]. The linear polarized electric field oriented in the z-direction provides an ideal environment to implement the highly orthogonal electric field distribution along different pathways.

B. *Pathway design procedure in the field generator*

The pathways used to perform the model validation test should meet the following criteria: (1) low correlations of electric fields along different pathways, which could be reflected by the low condition number of the complex matrix consisting of electric field along the validation pathway set; (2) generating high temperature rises for RF-induced heating so that better signal-to-noise ratio can be achieved in the measurement,\; and (3) mechanically achievable for AIMD.

The rows of the Hadamard matrix, whose entries are either +1 or -1, are mutually orthogonal. It has been widely employed in telecommunication and statistics. An example of an eighth-order Hadamard matrix is shown below:

$$\begin{bmatrix} 1 & 1 & 1 & 1 & 1 & 1 & 1 & 1 \\ 1 & -1 & 1 & -1 & 1 & -1 & 1 & -1 \\ 1 & 1 & -1 & -1 & 1 & 1 & -1 & -1 \\ 1 & -1 & -1 & 1 & 1 & -1 & -1 & 1 \\ 1 & 1 & 1 & 1 & -1 & -1 & -1 & -1 \\ 1 & -1 & 1 & -1 & -1 & 1 & -1 & 1 \\ 1 & 1 & -1 & -1 & -1 & -1 & 1 & 1 \\ 1 & -1 & -1 & 1 & -1 & 1 & 1 & -1 \end{bmatrix},$$

which is an 8 by 8 matrix with a condition number of 1. If one can find pathways along which the electric field can be mapped onto this matrix, the incident fields would then be orthogonal to each other. One way to realize pathways 2 and 3 in the matrix is shown in Fig. 3. By folding these pathways along the incident field direction, +1 and -1 in the matrix can be achieved.

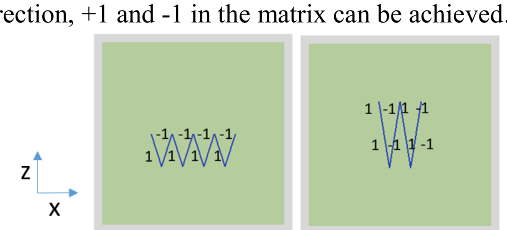

Fig. 3 The first two of seven pathways based on Hadamard matrix

However, these pathways fail to meet criterion (3), since bending the electrode along the pathway is very difficult in practice. To have relative smooth pathways with a still low correlated electric field, we propose to use the following pathway matrix as

$$\begin{bmatrix} 1 & 1 & 1 & 1 & 1 & 1 & 1 & 1 \\ 1 & 0 & 1 & 0 & 1 & 0 & 1 & 0 \\ 1 & 1 & 0 & 0 & 1 & 1 & 0 & 0 \\ 1 & 0 & 0 & 1 & 1 & 0 & 0 & 1 \\ 1 & 1 & 1 & 1 & 0 & 0 & 0 & 0 \\ 1 & 0 & 1 & 0 & 0 & 1 & 0 & 1 \\ 1 & 1 & 0 & 0 & 0 & 0 & 1 & 1 \\ 1 & 0 & 0 & 1 & 0 & 1 & 1 & 0 \end{bmatrix}.$$

Since the electric fields for both 1.5 T and 3 T are linearly polarized in the z-direction, 0 is equivalent to have the lead segment placed along the x-direction for the null electric field. The condition number of the revised matrix increases to 5.83, but the newly designed pathways can be easily achievable as shown in Fig. 4. The pathways corresponding to the first row were ignored since they are longer than the entire length of the test fixture.

For those AIMDs with different lengths, each segment length should be the total length divided by eight. Therefore, the revised Hadamard matrix can be treated as the design prototype of the validation pathway for the transfer function of the AIMDs.

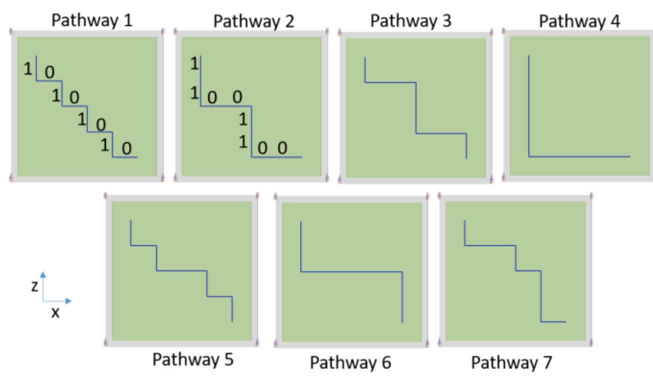

Fig. 4. The newly designed pathways following the revised matrix.

III. RESULT

A. *Two AIMDs validation tests*

To verify the feasibility of the proposed strategy, two generic AIMDs are used as examples. Both have a solid metal inner conductor with a radius of 0.4 mm. The inner conductors are coated by an outer silicon layer with a thickness of 0.4 mm. The relative permittivity of the silicon is 3.5. The lead lengths for the two AIMDs are 40 cm and 30 cm, respectively. Both AIMDs have a 5 mm bare lead tip at the distal end, and a dummy Implantable Pulse Generator(IPG) made with a copper sheet connected to a 2 Ω resistor at the proximal end. Based on the reciprocity theorem [14], the measured transfer functions are shown in Fig. 5.

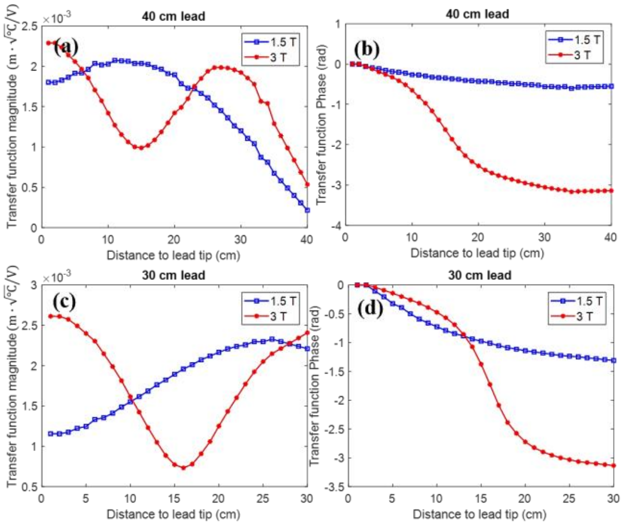

Fig. 5. The measured transfer functions of two example AIMDs for both 1.5 T (64 MHz) and 3 T (128 MHz). (a) Magnitude and (b) phase of the transfer function of a 40 cm AIMD; (c) Magnitude and (d) phase of the transfer function of a 30 cm AIMD.

The field generating system is shown in Fig. 6 (a). The resonator is loaded by a 9 cm height Polyacrylic Acid (PA A) gel with dielectric parameters of 0.47 S/m and 78, for conductivity and relative permittivity, respectively [22],[23]. Two AIMDs shown in Fig. 6(b) are placed at the central slice of the gel. The first validation pathway for the 40 cm AIMD is shown in Fig. 6(c). A plastic mesh is used to provide a stable fixation for the AIMDs. The temperature rise at the lead tip is recorded by the thermal optical probe, which is closely bonded onto the bare tip as shown in Fig. 6(d). The duration of each exposure test with the RF source on was 5 minutes.

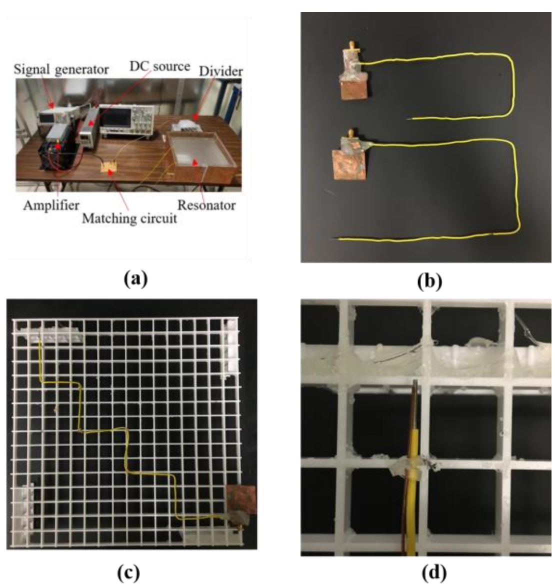

Fig. 6. (a) The whole electric field generator system. (b) Two generic AIMDs with different lengths. (c) The configuration of the first validation pathway for the 40 cm AIMD. (d) The bare lead tip and thermal optical probe in proximity.

The numerical software used in this study is SEMCAD X. The input power in the simulation is 32.52 W and 13.77 W for the 1.5 T and 3 T modes, respectively, so that the incident electric field at the central point in the resonator is same as the point which is 2 cm from the left wall of the ASTM phantom, and central with respect to the other two directions (This location is suggested by ASTM F2182 to test the RF heating caused by medical implants [24].) when the whole body SAR in the ASTM phantom is 2 W/Kg. The corresponding RMS values of the electric field are 115.2 V/m and 91.4 V/m, for the 1.5 T and 3 T units, respectively.

The measurement results were obtained with different power and normalized to the same input power as in the simulation (32.52 W and 13.77 W for the1.5 T and 3 T modes, respectively) by the calorimetry method, as suggested in the ASTM 2182 standard [24].

For the 40 cm AIMD, the simulated tangential electric field distributions along seven pathways are shown in Fig. 7. The condition numbers of the 1.5 T and 3 T electric field matrices are 3.41 and 4.23, respectively. The comparison of temperature rises obtained from direct measurements and that predicted by the transfer function method is shown in Fig. 8. For the 1.5 T validation tests, all of the pathways have a great fit with respect to criteria (2) since the highest background heating in the gel when the lead is absent during the same period is 0.47 ℃. For the 3 T test, with a background heating of 0.30 ℃, pathway 5 has the lowest SNR of 4.4 dB, except pathway 6, for which the predicted temperature rise (0.12 ℃) is lower than the background heating. That makes pathway 6 an ineffective validation test. From Equation 1, the temperature rise is the complex cumulation of the product of the transfer function and incident electric field. The low heating value is often related to field cancellation due to the phase shift. Overall, they are still good validation pathways based on the three pathway selection criteria.

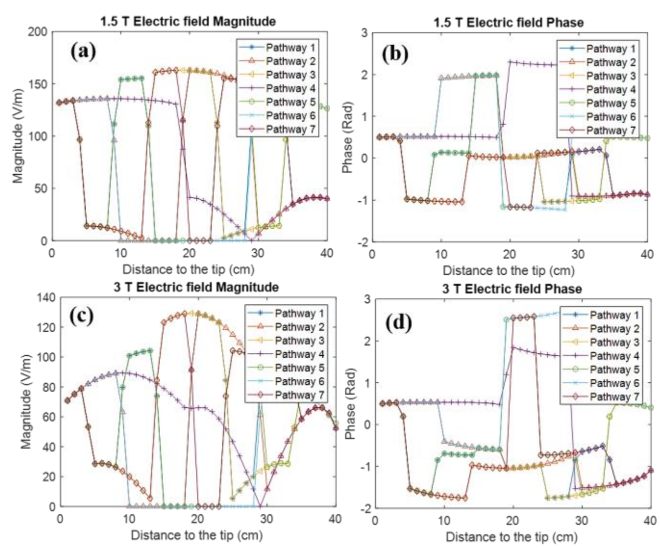

Fig. 7. Simulated electric field distributions along seven pathways shown in Fig. 4. (a) 1.5 T tangential electric field magnitude and (b) phase. (c) 3T tangential electric field magnitude and (d) phase.

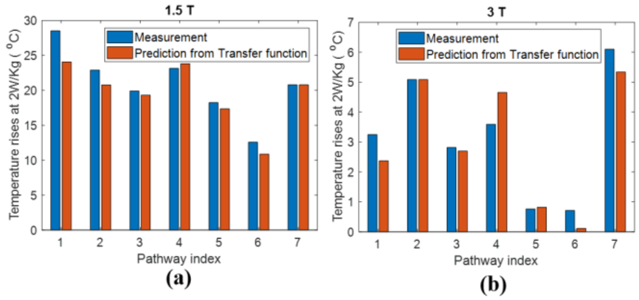

Fig. 8. Comparison of temperature rises at the lead tip electrode derived from measurement and the prediction by transfer function for 40 cm AIMD at (a) 1.5 T and (b) 3 T.

For the 30 cm AIMD, the pathways shown in Fig. 4 can still be applied for the 1.5 T transfer function validation, with the only change being a shortening of the single segment length from 5 cm to 3.5 cm. To minimize the influence of the fringing field, the middle point of the 30 cm AIMD should be at the central position in the resonator. The validation result for 1.5 T is given in Fig. 9 (a). The worst SNR appears in pathway 4, but it still larger than 10 dB. However, for the 3 T validation, the performance of the prototype pathway deteriorates dramatically, since pathways 1, 2 and 6 would have predicted temperature rises of (0.12, 0.25, and 0.12 ℃) which are similar to the background heating (0.30 ℃). Thus, further modification is needed for the 3 T test for the 30 cm AIMD.

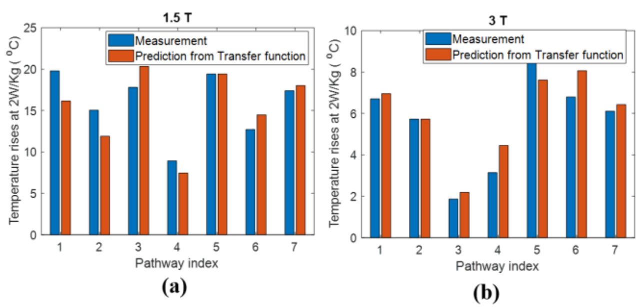

Fig. 9. Comparison of temperature rises at the lead tip electrode derived from measurement and the prediction by transfer function for the 30 cm AIMD. (a) 1.5 T using the prototype pathways in Fig. 4; (b) 3 T using the modified pathway shown in Fig. 10.

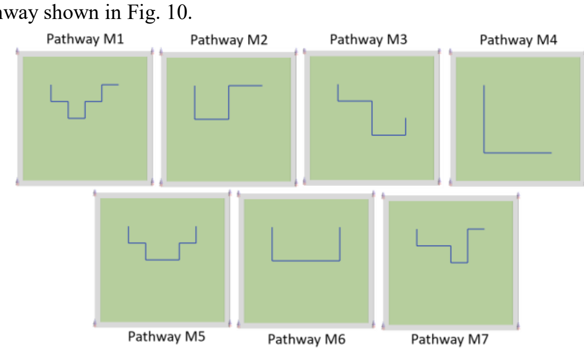

Fig. 10. Modified validation pathways for the 30 cm AIMD in the 3 T test.

Based on this argument, the z-directional segments in the second half of each pathway in Fig. 4 are flipped upward so that a reversed phase can be achieved. The modified pathways are illustrated in Fig. 10. The condition numbers of the 1.5 T and 3 T electric field matrices are 3.23 and 7.88, respectively. With the modified pathways, the SNR improved significantly. The validation result for the 3 T mode is shown in Fig. 9(b). The worst SNR (pathway 3) is higher than 8.6 dB.

B. Uncertainty analysis

Following the recommended strategy by ISO/TS 10974 Ed. 1 Annex R, the uncertainty in the validation test needs to be quantified using the GUM method [16], [25]. The uncertainty sources in this test can be categorized into two parts:

(1) The uncertainty from the transfer function model prediction, including the transfer function measurement.

(2) The uncertainty from the transfer function validation, including the numerical simulation and the temperature rise measurement. The proposed model (Equation 1) is a conservative calculation model for the temperature rises, since as the temperature of the tissue or the gel increases, both the specific heat and the thermal conductivity will rise [24], [26]. Therefore, the change in the thermal properties is also considered as an uncertainty source included in the "temperature rise measurement" part. More details can be found in the Appendix.

The uncertainty specification for the 1.5 T and 3 T tests is given in Table I and Table II. The combined plot of the measured and predicted temperature rises, as well as the uncertainty boundary, as shown in Fig. 11. It can be noticed that all measurement-prediction pairs locate within the $\Delta T(1 \pm 2\sigma) \pm 1$℃ region, for both the 1.5 T and 3 T tests.

TABLE I
UNCERTAINTY SPECIFICATION FOR 1.5 T TEST

1.5 T	Source of uncertainty	Uncertainty in %
Uncertainty for TF [a] model prediction	TF measurement	1.85
Uncertainty for TF model validation test	Temperature rise measurement	9.61± 1.0℃
	Numerical simulation	2.17
Combined Uncertainty	10.02± 1.0℃	

TABLE II
UNCERTAINTY SPECIFICATION FOR 3 T TEST

3 T	Source of uncertainty	Uncertainty in %
Uncertainty for TF model prediction	TF measurement	1.29
Uncertainty for TF model validation test	Temperature rise measurement	18.27± 1.0℃
	Numerical simulation	4.78
Combined uncertainty	18.92± 1.0℃	

[a] TF is the abbreviation for the transfer function.

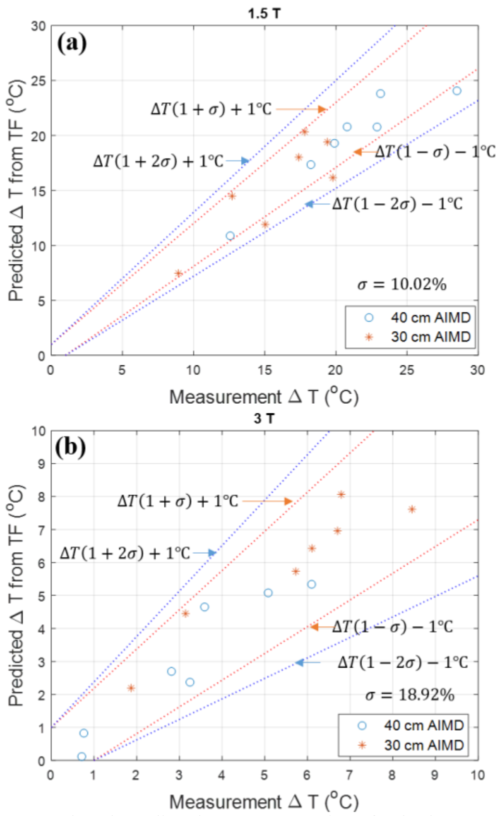

Fig. 11 Measured and predicted temperature rises for both AIMDs together with the uncertainty boundary for (a) 1.5 T, and (b) 3 T.

IV. DISCUSSION

The preceding case studies show that the proposed instrument can be an alternative system to perform RF-safety assessment for AIMDs. It has three main advantages over conventional RF coils.

(1) It is more compact due to the integration of the 1.5 T and 3 T cases.

(2) It has a more uniform electric field distribution which lowers the uncertainty due to the lead pathway shift.

(3) The electric fields along different pathways used in this strategy is more highly orthogonal to each other than those recommended by ISO 10974.

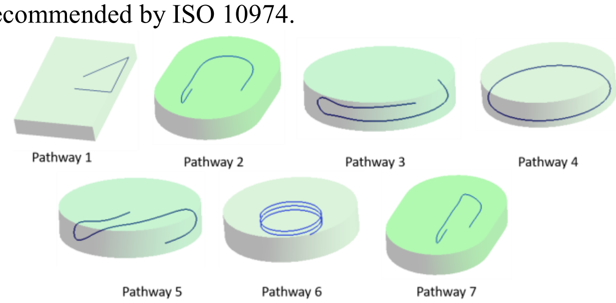

Fig. 12 The recommended validation pathways for AIMDs by ISO 10974

To demonstrate the second advantage, the uncertainty due to the lead pathway shift in an ASTM rectangular phantom and the proposed resonator is compared. For the ASTM phantom, the first three pathways of 40 cm in Fig. 4, are shifted in three directions by 10 mm, to obtain the predicted temperature rise perturbation using Equation 1. The transfer function is assumed to be constant. For the resonator, the same pathways are also shifted in three directions by 10 mm, to obtain the resulting change of calculated temperature rises. The average of three pathways' sensitivity coefficients in three directions and the combined results, as well as the uncertainty due to the shift of the pathway are given in Table III. It shows that the 3 T mode would be more sensitive to the effect of pathway shifting for both the proposed system and RF coils. However, due to the higher homogeneity of electric field distribution, the new system has superior performance on the uncertainty caused by pathway shifting at both frequencies.

TABLE III
THE UNCERTAINTY DUE TO THE SHIFT OF THE PATHWAYS FOR THE PROPOSED SYSTEM AND RF COIL AT 1.5 T AND 3 T

		Proposed system		RF coils	
		1.5 T	3 T	1.5 T	3 T
Sensitivity coefficients (/mm)	X direction	0.09	0.11	1.66	0.74
	Y direction	0.39	1.36	1.90	5.09
	Z direction	0.06	0.19	0.51	0.10
	Combination	0.41	1.38	2.57	5.14
Standard deviation of pathway shift		10 mm			
Uncertainty in %		4.06	13.79	25.68	51.44

TABLE IV
THE CONDITION NUMBERS OF THE INCIDENT ELECTRIC FIELD MATRIX EXTRACTED ALONG THE PROPOSED PATHWAYS IN THE RESONATOR AND THOSE RECOMMENDED ONES BY ISO 10974 IN RF COILS

	Proposed pathways	Recommended pathways by ISO 10974
1.5 T	3.41	118.63
3 T	4.23	71.54

To illustrate the third advantage, the correlation among the pathways presented in this paper and those recommended by ISO 10974, as shown in Fig. 12, are compared. The 40 cm pathways are used for comparison. The quadrature excitation mode for the 1.5 T and 3 T coils is selected. For seven validation pathway sets of the two methods, the condition numbers of the incident electric field matrix are given in Table IV. It shows that the electric field along the pathways used in this paper has significantly higher orthogonality than those recommended pathways used in RF coils for both working frequencies.

V. CONCLUSION

This paper proposes an efficient validation strategy for transfer functions for AIMDs. Applying a high electric field generating system and a set of validation pathways along which the electric field is orthogonal, this strategy could be an alternative to the recommended one in ISO 10974. There are three advantages of new strategy: first, it is more compact due to the integration of the 1.5 T and 3 T cases; second, it achieves lower uncertainty caused by the shift of pathways compared to a RF coil resulting from the higher electric field homogeneity; third, the orthogonality of the electric field along different pathways is significantly improved by a set of designed pathways inspired by the Hadamard matrix. From two AIMD studies, the prototype in Fig. 4 could provide initial pathways to perform the transfer function validation test. However, modification is potentially needed if the prototype does not satisfy design criterion (2), the SNR requirement.

APPENDIX

The detail of uncertainty analysis for the proposed system is shown as follows.

The uncertainty of type B is derived from the measurement instruments' specification for the NI network analyzer and temperature measurement system. To determine the uncertainty of type A, pairs of numerical simulations with only a single parameter variation have been executed. Two realistic values "V1", and "V2" are chosen for each variable as shown in Table VIII. A linear dependence of the measurement values on the changing parameter is assumed. The sensitivity factors f_i for each parameter can be determined. The standard deviation s_i is derived based on the measurements. The product of the sensitivity factor and the corresponding standard deviation is the uncertainty contribution of this parameter. The combined uncertainty at the 1sigma-level can be calculated using the formula $\sqrt{\sum(s_i f_i)^2}$.

TABLE V
THE UNCERTAINTY OF TRANSFER FUNCTION MEASUREMENT

Source of uncertainty	Uncertainty type	1.5 T Uncertainty in %	3 T Uncertainty in %
Mutual coupling between VNA ports	B	0	0
VNA drift	B	1.16	1.16
Liquid conductivity	A	1.41	0.19
Liquid permittivity	A	0.29	0.54
Combined Std.	-	1.85	1.29

TABLE VI
THE UNCERTAINTY OF TEMPERATURE RISES MEASUREMENT

Source of uncertainty	Uncertainty type	1.5 T Uncertainty in %	3 T Uncertainty in %
Liquid conductivity	A	7.56	11.38
Liquid permittivity	A	0.85	0.33
Leads path	A	4.06	13.79
Gel height	A	1.58	2.18
Liquid thermal conductivity	A	2.73	2.73
Liquid specific heat	A	1.36	1.36
Readout electronics	B	± 1.0℃	± 1.0℃
Combined Std.	-	9.61 ± 1.0℃	18.27± 1.0℃

TABLE VII
THE UNCERTAINTY OF NUMERICAL SIMULATION

Source of uncertainty	Uncertainty type	1.5 T Uncertainty in %	3 T Uncertainty in %
Grid resolution	A	2.08	0.80
Dielectric box relative permittivity	A	0.61	4.71
Combined Std.	-	2.17	4.78

TABLE VIII
THE DETAILS OF UNCERTAINTY SOURCE (UNCERTAINTY TYPE A ONLY)

Uncertainty category	Parameters	Quantity	V1	V2	Standard deviation	1.5 T Sensitivity factor	1.5 T uncertainty in %	3 T Sensitivity factor	3 T uncertainty in %
Transfer function measurement	Liquid conductivity	TF	0.47 S/m	0.517 S/m	0.033 S/m	42.69	1.41	5.69	0.19
	Liquid permittivity	TF	80	88	2.85	0.10	0.29	0.19	0.54
Numerical simulation	Grid resolution	E_{incid}	2 mm	4 mm	2 mm	1.04	2.08	0.40	0.80
	Dielectric box relative permittivity	E_{incid}	2.25	3	0.75	0.81	0.61	6.28	4.71
Tempera-ture rises measurement	Liquid conductivity	E_{incid}	0.47 S/m	0.517 S/m	0.033 S/m	229.11	7.56	344.86	11.38
	Liquid permittivity	E_{incid}	80	88	2.85	0.30	0.85	0.12	0.33
	Liquid thermal conductivity	T	0.42 W/(m·k)	0.5 W/(m·k)	0.02 W/(m·k)	136.67	2.73	136.67	2.73
	Liquid specific heat	T	4159 J/(kg·k)	4206 J/(kg·k)	160 J/(kg·k)	0.01	1.36	0.01	1.36
	Leads path	E_{incid}	0 mm	10 mm	10 mm	0.41	4.06	1.38	13.79
	Gel height	E_{incid}	9 cm	9.5 cm	0.2 cm	7.92	1.58	10.89	2.18

REFERENCES

[1] S. M. Park, R. Kamondetdacha, A. Amjad, and J. A. Nyenhuis, "MRI safety: RF-induced heating near straight wires," *IEEE Trans. on Magn.*, vol. 41, no. 10, pp. 4197–4199, 2005.
[2] C. J. Yeung, P. Karmarkar, and E. R. McVeigh, "Minimizing RF heating

of conducting wires in MRI," *Magn. Reson. Med.*, vol. 58, no. 5, pp. 1028–1034, 2007.

[3] C. E. McElcheran, B. Yang, K. J. T. Anderson, L. Golenstani-Rad, and S. J. Graham, "Investigation of parallel radiofrequency transmission for the reduction of heating in long conductive leads in 3 Tesla magnetic resonance imaging," *PLoS One*, vol. 10, no. 8, pp. 1–21, 2015.

[4] C. Armenean, E. Perrin, M. Armenean, O. Beuf, F. Pilleul, and H. Saint-Jalmes, "RF-induced temperature elevation along metallic wires in clinical magnetic resonance imaging: Influence of diameter and length," *Magn. Reson. Med.*, vol. 52, no. 5, pp. 1200–1206, 2004.

[5] V. Acikel and E. Atalar, "Modeling of radio-frequency induced currents on lead wires during MR imaging using a modified transmission line method," *Med. Phys.*, vol. 38, no. 12, pp. 6623-6632, 2011.

[6] A. Missoffe, J. Kabil, P. A. Vuissoz, and J. Felblinger, "Transmission line model of an implanted insulated cable for magnetic resonance imaging radiofrequency hazard evaluation," *IEEE J. Electromagn. RF Microwaves Med. Biol.,* vol. 2, no. 3, pp. 201 - 207, 2018.

[7] J. Liu *et al.*, "Investigations on Tissue-Simulating Medium for MRI RF Safety Assessment for Patients With Active Implantable Medical Devices," *IEEE Trans. on Electromagn. Compat.*, 2018.

[8] J. Liu, J. Zheng, Q. Wang, W. Kainz, and J. Chen, "A Transmission Line Model for the Evaluation of MRI RF-Induced Fields on Active Implantable Medical Devices," *IEEE Trans. Microw. Theory Tech.*, vol. 61, no. 4, pp. 1091 - 1097, 2019.

[9] Y. Wang *et al.*, "On the development of equivalent medium for active implantable device radiofrequency safety assessment," *Magn. Reson. Med.*, vol. 82, no. 3, pp. 1164-1176, 2019.

[10] E. Mattei, G. Calcagnini, F. Censi, M. Triventi, and P. Bartolini, "Role of the lead structure in MRI-induced heating: In vitro measurements on 30 commercial pacemaker/defibrillator leads," *Magn. Reson. Med.*, vol. 67, no. 4, pp. 925–935, 2012.

[11] E. Mattei *et al.*, "Complexity of MRI induced heating on metallic leads: Experimental measurements of 374 configurations," *Biomed. Eng. Online*, vol. 7, pp. 1–16, 2008.

[12] S. M. Park, R. Kamondetdacha, and J. A. Nyenhuis, "Calculation of MRI-induced heating of an implanted medical lead wire with an electric field transfer function," *J. Magn. Reson. Imaging*, vol. 26, no. 5, pp. 1278–1285, 2007.

[13] S. Feng, R. Qiang, W. Kainz, and J. Chen, "A technique to evaluate MRI-induced electric fields at the ends of practical implanted lead," *IEEE Trans. Microw. Theory Tech.*, vol. 63, no. 1, pp. 305–313, 2015.

[14] Q. Zeng, Q. Wang, J. Zheng, W. Kainz, and J. Chen, "Evaluation of MRI RF electromagnetic field induced heating near leads of cochlear implants," *Phys. Med. Biol.*, 63 135020, 2018.

[15] U. Zanovello, M. Borsero, D. Giordano, L. Zilberti, F. Maggiorelli, and G. Tiberi, "Experimental setup to compare measurements and numerical simulations in magnetic resonance imaging RF dosimetry," *IEEE Trans. on Instrum. and Meas.*, vol. 66, no. 6, pp. 1208 - 1216, 2017.

[16] Assessment of the safety of magnetic resonance imaging for patients with an active implantable medical device, ISO/TS 10974 ED2, March, 2016.

[17] E. Schock, "What are the proper condition numbers of discretized III-posed problems?," *Linear Algebra Appl.*, vol. 81, no. C, pp. 129–136, 1986.

[18] R. A. Horn and C. R. Johnson, *Topics in matrix analysis*. 1991.

[19] L. Streeter, G. R. Burling-Claridge, M. J. Cree, and R. Künnemeyer, "Optical full hadamard matrix multiplexing and noise effects," *Appl. Opt.*, 2009.

[20] G. Kou, D. Ergu, and J. Shang, "Enhancing data consistency in decision matrix: Adapting Hadamard model to mitigate judgment contradiction," *Eur. J. Oper. Res.*, 2014.

[21] S. Song, *et al.,* "Multi-Frequency High Electric Field System forMRI Safety Test of Implantable Medical Devices", to be published.

[22] J. Baker-Jarvis, M. D. Janezic, and C. A. Jones, "Shielded open-circuited sample holder for dielectric measurements of solids and liquids," *IEEE Trans. Instrum. Meas.*, vol. 47, no. 2, pp. 338–344, 1998.

[23] M. A. Stuchly, M. A. Stuchly, and S. S. Stuchly, "Coaxial Line Reflection Methods for Measuring Dielectric Properties of Biological Substances at Radio and Microwave Frequencies—A Review," *IEEE Trans. Instrum. Meas.*, vol. 29, no. 3, pp. 176–183, 1980.

[24] ASTM F 2182-11a. Standard test method for measurement of radio frequency induced heating near passive implants during magnetic resonance imaging. ASTM Committee F04 on Medical and Surgical Materials and Devices, Subcommittee F04.15 on Material Test Methods. West Conshohocken, PA: ASTM International; 2011.

[25] P. Da Silva Hack and C. S. Ten Caten, "Measurement uncertainty: Literature review and research trends," *Trans. Instrum. Meas.,* vol. 61, no. 8, pp. 2116–2124, 2012.

[26] Bhattacharya, Anandaroop & Mahajan, Roop. (2003). Temperature dependence of thermal conductivity of biological tissues. Physiological measurement. 24. 769-83. 10.1088/0967-3334/24/3/312